

Optimizing Feed Modulation for Coupled Methane and NO_x Conversion over Pd-Pt/Mn_{0.5}Fe_{2.5}O₄/Al₂O₃ Monolith Catalyst

Kyle Karinshak¹, Pak Wing Chen¹,

Ru-Fen Liu², Stephen J. Golden³, Michael P. Harold^{1*}

¹William A. Brookshire Department of Chemical and Biomolecular Engineering,
University of Houston, Houston, Texas 77204, USA

²CDTi Advanced Materials, Inc., 1641 Fiske Place, Oxnard, California 93033, USA

³Formerly with CDTi Advanced Materials, Inc.; now with INTERKAT Catalyst GmbH,
53639 Königswinter, Germany

*Corresponding author: mpharold@central.uh.edu

ABSTRACT: The impacts of feed modulation (frequency, amplitude) and catalyst design (composition and architecture) parameters are reported for the conversion of methane and NO_x over a dual-layer Pt+Pd/Al₂O₃ + Mn_{0.5}Fe_{2.5}O₄/Al₂O₃ monolith. CH₄ and NO_x conversion data show that the dual-layer catalyst outperforms single-layer samples having the same catalyst loadings, with and without spinel. Close proximity of the PGM and MFO functions in the mixed-layer catalyst lowers the CH₄ conversion at high temperature while separating the PGM and spinel layers with an intermediate Al₂O₃ layer does not. Methane conversion enhancement is linked to its nonmonotonic dependence on O₂. The performance gains are tied to a transient activity spike that occurs during the lean-to-rich feed transition when water is present in the feed. The transient spike is attributed to the removal of CO and H₂ products via reactions with stored O₂ in the spinel, eliminating inhibition of methane steam reforming.

Keywords: Methane oxidation; NO_x reduction; Platinum; Palladium; Spinel;

1. Introduction

There is increased global attention in greenhouse gas (GHG) emissions and the need to curtail their growth. Vehicular emissions were responsible for 24% of GHG emissions in the USA during 2017 [1]. This has prompted a closer look at Natural Gas Vehicles (NGVs) as a lower GHG alternative for medium- and heavy-duty applications. With the primary constituent of abundant NG being methane (CH_4), NG has a higher H:C ratio than gasoline or diesel and therefore its combustion produces less CO_2 . However, CH_4 is itself a more potent greenhouse gas than CO_2 with a GHG potential about 25 times that of CO_2 [2]. For this reason, uncombusted CH_4 in NGV exhaust must be eliminated in order to clear the way for the growth in the NGV market.

The conventional Three-Way Catalyst (TWC) used for stoichiometric gasoline engine emission control is ineffective for CH_4 oxidation. Current stoichiometric NGVs use modified TWCs with a rather high loading of Platinum Group Metal (PGM) – upwards of 200 g PGM/ft³ – in order to meet emission targets [3]. Given the high cost of PGM, catalysts with lower PGM loading are critically needed. Recent research has shown that lean/rich feed modulation can enhance TWC performance for CH_4 conversion [4–11]. Shi et al. [12] reported increased CH_4 conversion when switching from a steady to oscillating (modulating) air-to-fuel (lean/rich) ratio. Ferri et al. [10] showed that periodic lean/rich switching during methane oxidation on a Pd-based TWC that the conversion maximum could be increased with increasing amplitude. The location of the maximum occurred in the rich regime. The investigators noted, importantly, that the methane abatement efficiency benefits from control of the switching sequence. In addition to feed modulation, there is a large corpus of research

demonstrating the beneficial effects of dopants, bimetallics, and oxygen storage materials (OSMs) on TWC methane oxidation activity [13–17]. The contemporary TWC applied to NGVs is typically bimetallic (usually Pt + Pd) and contains ceria-zirconia (CZO; $\text{CeO}_2\text{-ZrO}_2$) to achieve high conversions of CO, NO, and CH_4 . The role of the ceria is to mitigate fluctuations (dithering) in the air-to-fuel ratio brought about by lambda (λ) control, enabling high conversion of CO, NO, and hydrocarbons (HCs). The OSM works through a redox reaction scheme to store and release oxygen during the lean and rich conditions, respectively [18,19].

In recent years there has been interest in the use of mixed metal oxides with the ordered spinel structure AB_2O_4 serving as the OSM in tandem with a PGM component or as a standalone catalyst. Fino et al. [20,21] reported that the addition of CoCr_2O_4 to Pd-based catalysts improves the catalytic conversion of CH_4 . Given that their experiments were conducted using a feed devoid of H_2O and CO_2 , it is of interest to learn of the generality of their findings with more realistic feeds. In our recent work we demonstrated that the addition of the $\text{Mn}_{0.5}\text{Fe}_{2.5}\text{O}_4$ (MFO) spinel to a Pt-rich bimetallic (with Pd) catalyst resulted in enhanced CH_4 oxidation under modulating feed conditions [22]. The combination of modulation and the added spinel gave higher CH_4 and NO conversions than either modulating feeds or the addition of spinel alone. These spinel-enhanced TWCs are called Four Way Catalysts (FWCs) for their ability to eliminate NO_x ($x = 1, 2$), CO, non-methane hydrocarbons (NMHCs), and CH_4 .

Our previous study demonstrated enhanced methane oxidation activity with the addition of spinel (MFO) to Pt/Pd along with lean/rich feed modulation. However, that study did not systematically examine the impact of modulation, and while some

speculative explanations were advanced, the root cause for the enhanced activity is inconclusive. To this end, in the current study we examine the impact of dual-function spinel MFO + Pt/Pd catalyst composition and architecture, along with modulation parameters on catalyst performance. The results reveal an impressive enhancement in CH₄ and NO conversion with the best results obtained over finite ranges of amplitude and frequency. Further, the transient CH₄ conversion during specific lean-to-rich feed transitions provide compelling evidence for the underlying mechanism responsible for the enhanced methane oxidation activity. Finally, the observed conversion enhancements improve when separation exists between the spinel and the PGM. To this end, a root-cause mechanism is advanced that explains the collection of measurements.

2. Materials and Methods

Washcoated monolith samples were provided from CDTi (Oxnard, CA). The baseline catalyst has a dual-layer design loaded onto a 600 cpsi (cells per square inch) cordierite monolith [22]. The first washcoat is Al₂O₃-supported Mn_{0.5}Fe_{2.5}O₄ (MFO) Spinel™ (25 wt.%). A second washcoat of 30 g/ft³ PGM (19:1 Pt to Pd mass ratio) supported on Al₂O₃ is deposited on top of the Spinel/Al₂O₃ layer. Both layers have a total loading of 100 g/L. Measurement (Micromeritics 3 Flex apparatus) of CO chemisorption on the PGM/Al₂O₃ powder (used in the single- and dual-layer catalysts) gave a PGM dispersion of 13%. Variations of the baseline catalyst design were also synthesized in order to test specific catalyst features; namely, the PGM-Only catalyst, single-layer PGM-Only catalyst, single-layer PGM+Spinel catalyst, and three-layer

catalysts containing an intermediate Al_2O_3 layer of varying loading (thickness). Figure 1 provides schematics of the five catalyst designs. The PGM-Only catalyst has the same dual-layer structure and loadings as the PGM+Spinel catalyst, but the bottom layer is pure Al_2O_3 . The single-layer PGM-Only catalyst has the bottom pure Al_2O_3 layer removed, and thus has a total loading of only 100 g/L. The single-layer PGM+Spinel catalyst is a variant of the PGM+Spinel baseline sample, wherein the two distinct layers have instead been mixed into one uniform washcoat; for this sample, the PGM was impregnated directly into the $\text{Mn}_{0.5}\text{Fe}_{2.5}\text{O}_4/\text{Al}_2\text{O}_3$. Finally, the intermediate layer catalysts have the same PGM and MFO loadings as the baseline PGM+Spinel, but with lower washcoat loadings of 60 g/L each. In between the PGM and the MFO layers, an intermediate washcoat of Al_2O_3 was added with three different loadings: 40 g/L, 60 g/L, and 80 g/L. These intermediate layers separate the PGM function from the MFO function by an estimated $\sim 14\ \mu\text{m}$, $\sim 21\ \mu\text{m}$, and $\sim 28\ \mu\text{m}$, respectively.

Experiments were carried out in two reactor systems with somewhat different features and physical locations. The first reactor system located at the University of Houston (UH) is described in detail in our previous paper [22]. The second reactor system located at CDTi has a similar overall design as the UH reactor with some distinct differences; whereas the UH reactor system has a single four-way switching valve to modulate the O_2 feed concentration, there are two three-way valves in the CDTi system are controlled through Labview™. Experiments at the two laboratories also employ slightly different operating conditions and monolith core sizes. At UH, a gas hourly space velocity (GHSV) of 40k hr^{-1} was used in conjunction with cores 1" diameter by 0.82" length, whereas CDTi experiments were conducted at GHSV of 90k hr^{-1} . Further,

different temperature ramp rates were utilized during light-off experiments: 10 °C/min at UH and 40 °C/min at CDTi. Experimental sets repeated by both labs showed the same trends regardless of space velocity and temperature ramp rate. Finally, it is noted unless otherwise specified, the varied “temperature” in the light-off experiments corresponds to the feed temperature. Given the strongly exothermic CO, H₂, and CH₄ oxidation reactions occurring across the length of the reactor, temperature gradients between the inlet and outlet of the catalyst can be as high as 85 °C are observed.

All pretreatments are summarized in Table 1. Except when specifically testing the effects of various pretreatment parameters, catalyst samples were preheated at 525 °C under slightly-rich, feed modulated conditions for 30 minutes (listed as “Modulation Pretreatment” in Table 1.) Experiments conducted by CDTi were subject to a similar pretreatment with slightly more H₂ and O₂, listed in Table 1 as “CDTi Pretreatment”. Catalysts were tested under a variety of modulated and non-modulated feed conditions depending upon the objectives of the experiment; these are summarized in Table 2. Which feed conditions were utilized for which experiments are specified in the Results section. The degree to which feed conditions are considered rich or lean is quantified by the lambda (λ) parameter, the ratio of oxidants to reductants, and is defined as follows:

$$\lambda = \frac{0.5 [(CO)+2(O_2)+(NO)+ (H_2O)+ 2(CO_2)]}{[(CO)+ (CH_4)+ (CO_2)]+ 0.25 [2(H_2)+4(CH_4)+ 2(H_2O)]} \quad (1)$$

Modulation involves feed switching abruptly from rich to lean conditions, and therefore necessitates several more parameters of interest. The “average lambda”, denoted by <λ>, is the cycle-average lambda of the feed, and was explored in our earlier work [22]. The “modulation amplitude” (A = 2Δλ ; dimensionless) is a measure of how far the rich

and lean phase compositions deviate from the cycle average lambda; i.e. $\lambda(t) = \langle \lambda \rangle + \Delta\lambda(t) = \langle \lambda \rangle + A(t)/2$. Finally, the “modulation frequency” (f; in Hz) is a measure of the cycling rate.

Some additional details are needed to fully describe the modulation parameter experiments. These experiment sets are as follows.

Modulation Amplitude Experiments: Modulation amplitude experiments conducted at CDTi had the average lambda and modulation frequency fixed at $\langle \lambda \rangle = 0.996$ and $f = 1$ Hz, respectively. The amplitude was fixed at 9 discrete values between $A = 0$ (no modulation) and 0.056. The $\langle \lambda \rangle$ values are as follows: 0.0, 0.0035, 0.007, 0.0105, 0.014, 0.021, 0.028, 0.042, and 0.056. A subset of these modulation amplitudes – 0.0, 0.007, 0.014, and 0.028 – were selected for experiments conducted at UH. The UH experiments had a feed that was slightly more rich ($\langle \lambda \rangle = 0.992$) and cycled more slowly ($f = 0.33$ Hz).

Modulation Frequency Experiments: Modulation frequency experiments occurred at fixed temperatures, rather than under temperature ramping conditions. The modulation amplitude was fixed at 0.028, 0.014, and 0.007 while $\langle \lambda \rangle$ was fixed at 0.992. Five frequencies were examined: 0.33, 0.25, 0.17, 0.07, and 0.05 Hz. An additional set of experiments explored a frequency of 0.0021 Hz, corresponding to a period of 480 s for a single lean/rich cycle, to better understand what occurred during the transitions between the rich and lean phases.

3. Results and Discussion

3.1 Catalyst Structure Effects

Our earlier study reported enhanced performance with a dual-layer PGM+Spinel catalyst [22]. Conventionally, the PGM and OSM functions are, by design, placed in close proximity to promote the oxygen storage/release and metal-OSC interactions [23]. Here we directly compare the dual-layer and single-layer PGM+Spinel catalysts in a temperature ramp light-off experiment using the CDTi modulating feed conditions ($\langle \lambda \rangle = 0.996$, $A = 0.028$, $f = 1$ Hz; Table 2). Fig. 2 shows that the dual-layer catalyst significantly out-performs the single-layer catalyst. There is nearly a 100 °C difference in the T_{50} values between the two catalysts. [T_{50} is the temperature at which 50% CH_4 conversion is obtained.] Additionally, not only does the dual-layer catalyst light off earlier, it also reaches and maintains a higher final CH_4 conversion. These results suggest that the spinel enhances the catalytic activity through a different mechanism than a conventional OSM CeO_2 -based material. That is, whereas CeO_2 (or $\text{CeO}_2+\text{ZrO}_2$) typically needs close proximity to the PGM for optimal performance, the MFO spinel requires some degree of separation from the PGM [24,25]. Additional data are presented below that highlight the differences between MFO spinel and CeO_2 , including the effects of an intermediate layer loading and the modulation frequency.

The dual-layer design provides benefits even when MFO spinel is not present. Figure 2 also shows the results of the single-layer and the dual-layer PGM-Only catalysts. For the latter sample a “dummy” layer of Al_2O_3 is present underneath the PGM-layer. Although the light-off commences at about the same temperature of ~ 300 °C, there is a 35 °C difference in the T_{50} between the two samples. The dual-layer design also reaches full conversion at a temperature of 60 °C lower the single-layer

catalyst. These improvements in CH₄ conversion for PGM-Only catalysts likely result from a corner-filling effect. That is, the bottom Al₂O₃ layer of the dual-layer samples fill the corners of the square monolith cross-section [26,27]. As a result, the top PGM layer has a more uniform thickness, enabling a better utilization of the PGM. Additionally, the overall higher loading of the dual-layer catalysts when compared to the single-layer catalysts results in a lower residence time for the same flowrate. Collectively, these data suggest that CH₄ oxidation is limited to some extent by washcoat diffusion [26,27]. Otherwise, the two catalysts would have identical conversions since they have identical PGM loadings. Finally, it is noted that the dual-layer PGM-Only catalyst is outperformed by the dual-layer PGM+Spinel catalyst. This underscores the enhancing role of the MFO spinel in promoting the oxidation.

An additional finding is evident when comparing the performance of the dual-layer PGM+Spinel and single-layer PGM+Spinel samples. Fig. 2 shows the single-layer PGM+Spinel has a much lower activity than its dual-layer counterpart as seen by their respective T₅₀ values and the CH₄ conversion at high temperature. These results suggest that there is active inhibition of the PGM by MFO when the two materials are mixed together. In our earlier study [22], we noted that the presence of spinel reduces the apparent activity of the dual-layer catalyst at high temperatures. Then we speculated that a negative interaction occurs between the spinel and PGM at the interface between catalyst layers could be responsible. More recent experiments with intermediate Al₂O₃ layer samples – to be shown next – indicates that another factor is responsible. A parallel study currently underway in our group suggests that the MFO spinel itself inhibits high temperature CH₄ conversion through the migration of base

metal/base metal oxide species to the PGM-layer. These Fe species deactivate PGM-active sites, leading to the inhibition of the Steam Methane Reforming (SMR) reaction. This effect is likely exacerbated when the MFO and PGM are in close proximity than we would need. We will communicate these findings in a future publication.

Experiments with intermediate-layer catalysts further demonstrate differences in the PGM + OSM proximity effect between MFO and a conventional OSM like CeO₂. The series of catalyst samples containing dummy layers of Al₂O₃ of varying thickness between the MFO and PGM layers enable a systematic examination of the importance (or lack of) of proximity between the two functions. Figure 3 reports the performance of this series of catalysts under modulated and non-modulated feed conditions. The data reveal that the intermediate layer has a negligible effect on the methane conversion. The sample with the 40 g/L intermediate layer loading only slightly out-performs the other catalysts; i.e., the T₅₀ for this catalyst is about ~8 °C lower than the rest of the samples under modulating conditions. For a time-invariant feed, the difference in T₅₀ values is ~15 °C. We attribute these small differences to experimental variations. The 60 g/L and 80 g/L intermediate layer catalysts have a higher conversion above 400 °C than the 0 g/L and 40 g/L intermediate layer catalysts under modulating conditions. This may be a result of the corner filling effect discussed earlier. These results are consistent in both of the reactor systems having different catalyst size and operating condition differences. There is almost certainly an intermediate layer loading that would decouple the spinel from the PGM functions. However, these Fig. 3 results indicate that loading exceeds 80 g/L. Later we examine in more detail the underlying mechanism principally responsible for the CH₄ conversion enhancement. This mechanism involves

diffusion of reacting species CO and H₂ through the washcoat layers. The negligible dependence of the Al₂O₃ layer loading suggests that the diffusion time through an intermediate layer with a loading as large as 80 g/L is small enough so as not to adversely impact the observed conversion enhancement during modulation. We will return to this issue later.

Based on results presented thus far, the dual-layer spinel + PGM catalyst design is clearly the best of those evaluated. The two layers minimize an apparent inhibitory effect of MFO on PGM activity, while also providing a moderate increase in activity due to the corner filling effect. As we expand on later, the MFO spinel specifically and spinels more generally have oxygen storage properties that contribute to the significant enhancement in methane oxidation performance and are distinguished from conventional OSM ceria.

3.2 Feed Parameter Effects

The PGM+ Spinel catalyst performance can be improved through optimization of the conventional operating conditions such as the feed composition, temperature and flow rate feed, and the less conventional parameters such as amplitude and frequency associated with feed modulation. In our previous study, we studied the impact of the average feed composition, or average lambda ($\langle\lambda\rangle$). Those results showed that $\langle\lambda\rangle$ has a significant effect on the performance of PGM-Only and PGM+Spinel catalyst performance. In particular, the CH₄ and NO conversions are highest under slightly-rich conditions due to a favorable coupling between the time-varying feed composition and the nonmonotonic dependence of methane conversion on the O₂ concentration. As we

show in this section, in addition to $\langle \lambda \rangle$, the modulation amplitude (A) and frequency (f) are important parameters that can be optimized.

3.2.1. Pretreatment

The effect of pretreatment on the PGM-Only and PGM+Spinel catalysts under modulating conditions was examined. Three different pretreatments were tested and are summarized in Table 1. The catalyst under study was treated with the different feed gas compositions at 525 °C for 30 minutes before conducting a standard light-off experiment under the full-feed modulation conditions ($\langle \lambda \rangle = 0.992$, $A = 0.028$, $f = 0.33$ Hz; Table 2). The first pretreatment type comprised modulation at the same conditions as the light-off experiment while the second and third feed modes had fixed (constant), net reducing ($\lambda = 0.992$) and net oxidizing ($\lambda = 1.038$) conditions. It has been previously shown that mixtures of metallic and oxidized PGM can be more active than entirely reduced or oxidized PGM alone. By subjecting the catalyst to modulation prior to the experiment, a favorable PGM mixture is achieved [28–30].

Figure 4 show the outcome of three different pretreatment types on the PGM-Only catalyst (4(a)) and PGM+Spinel catalyst (4(b)). For each of the catalysts, the modulated pretreatment leads to the most active catalyst based on the T_{50} value. We speculate that the modulating pretreatment results in the PGM crystallites on both the PGM-Only and PGM+Spinel samples having a blend of metallic and oxidized sites. This effect is reflected in a decreased T_{50} of ~35 °C for both catalysts. At higher temperatures, the conversion difference between the three pretreatments decreases. Interestingly, there is no significant difference between the net reducing and oxidizing pretreatments on the CH_4 conversion. Finally, a comparison of the PGM-Only and

PGM+Spinel samples indicates a more widely varying instantaneous CH₄ conversion for the former than the latter. This feature was found to hold throughout the study and is attributed to a lack of OSC functionality in the PGM-Only catalyst. This difference reflects the influence of the spinel in storing and releasing oxygen, thereby suppressing large swings in the conversion. OSMs are known to have this effect during modulating feed conditions; the spinel is functioning as other OSMs do, despite operating through a different mechanism.

3.2.2. Modulation Amplitude

Modulation amplitude experiments on the PGM-Only and PGM+Spinel catalysts were conducted by both CDTi and UH. For the CDTi experiments, the average lambda was fixed at 0.996 while the amplitude was set at 9 discrete values between and including $A = 0$ and 0.056. The corresponding lean and rich oxygen concentrations for each A value are shown in Table 2 along with other conditions.

The CH₄ conversion as a function of temperature data for the PGM-Only and PGM+ Spinel catalysts are shown in Fig. 5(a) and 5(b), respectively. It is noted that the somewhat “jagged”, non-monotonic nature of the light-off curves is a result of a combination of the rather high temperature ramp rate (40 °C/min) and the fast modulation frequency ($f = 1$ Hz). Each of the curves has the expected sigmoidal shape traversing the low temperature, low conversion regime to the high temperature, high conversion regime. For the PGM-Only sample, the CH₄ light-off commences (under non-modulated feed conditions, $A = 0$) at ~390 °C, reaches 50% conversion (T_{50}) at ~415 °C, and full conversion by ~430 °C. At low but non-zero modulation amplitudes up to $A = 0.014$, moderate increases in the CH₄ conversion are observed at all

temperatures with the T_{50} decreasing to ~ 380 °C. However, starting at $A=0.021$ the light-off curve features shift to a more gradual approach to the high conversion limit. So, while the light-off temperature continues to decrease, the T_{50} value goes through a local minimum of ~ 355 °C at an intermediate A value of 0.028. The nonmonotonic dependence causes the curves to overlap at higher temperatures and conversions. The decrease in the CH_4 conversion at temperatures exceeding ~ 390 °C is such that full conversion is not achieved until 500 °C, an increase of ~ 70 °C from the no-modulation result. In fact, for the highest amplitude considered ($A = 0.056$) the conversion decreases at all temperatures from the values obtained for $A = 0.042$.

The corresponding data for the PGM + Spinel catalyst in Fig. 5(b) show that the addition of Spinel eliminates the high temperature activity decline obtained for the PGM-Only catalyst (Fig. 5(a)). In contrast, a monotonic increase in the CH_4 conversion is obtained between $A = 0$ and 0.042. It is not until $A = 0.056$ that there is any indication of a conversion plateau or decrease. An overall comparison of the PGM-Only and PGM+Spinel data reveals a lower light-off temperature (T_{50}) for the former than the latter for non- and weakly-modulated feeds ($A = 0$ to ~ 0.014) and temperatures below 400 °C. That is, addition of the spinel apparently leads to a moderate decrease in catalytic activity. On the other hand, at higher amplitudes ($0.021 \leq A \leq 0.056$) the spinel has a noted enhancing effect. The experiments conducted at CDTi involved a faster temperature ramp (40 °C/min). This undoubtedly resulted in a more pronounced temperature gradient in the monolith and a higher conversion. Similar experiments conducted at UH involving a 10 °C/min ramp did not have as pronounced a difference in the conversions obtained for the two catalysts; see Fig. 6, described next. Moreover,

steady-state (no ramp) experiments conducted in our earlier study [22] showed much smaller differences in the light-off temperatures of the two catalysts.

The smaller set of varied amplitude experiments that were conducted at UH mostly confirm (Fig. 6) the main trends of the amplitude variation data shown in Fig. 5. Fig. 6 compares the effect of A for both the PGM-Only (a – c) and PGM+Spinel catalysts (d – f). Figs. 6(a) and (d) compare the CH₄ conversion, 6(b) and (d) the NO conversion, and (c) and (e) the NH₃ effluent concentration. Before dissecting these data, it is noted that in addition to a slower temperature ramp, the UH experiments had a lower space velocity, lower average lambda, and slower frequency. Thus, exact reproduction of the CDTi results is not expected. For instance, the CDTi data (Fig. 5) show complete conversion of CH₄ with the PGM+Spinel catalyst above 460 °C, whereas experiments conducted at UH (Fig. 6) show a conversion of ~90% at temperatures above 460 °C. We attribute the better performance obtained in the CDTi experiments to the faster temperature ramp (40 °C/min vs. 10 °C/min), producing an overshoot in CH₄ conversion.

Figure 6 shows additional performance data. As presented in our earlier work [22], the general trend for NO conversion is that it follows the CH₄ conversion since catalytic NO reduction is more effective at lower O₂ concentration. The sharp increase in NO conversion from the local minimum to complete conversion, seen for three of the cases in Figs. 6(b) and (e), occurs nearly coincidentally with the sharp increase in CH₄ conversion seen in Figs. 6(a) and (d). On the other hand, the more gradual increase in the CH₄ conversion for the PGM-Only, A = 0.028 case leads to a more gradual increase in NO conversion which does not exceed 80%. Addition of the spinel largely eliminates

this loss of performance evident in the PGM-Spinel data. NH_3 production occurs in two regimes; at temperatures below 225 °C and at temperatures above 350 °C. Low temperature NH_3 production is unaffected by modulation amplitude, but is affected by the presence of the MFO spinel. In the higher temperature regime, the NH_3 yield increases with increasing modulation amplitude, and NH_3 production begins at lower temperatures. The presence of spinel, as it does for CH_4 and NO conversion, largely eliminates the transient swings at higher modulation amplitudes. Finally, CO conversion, NO_2 production, and N_2O production are negligibly affected by changes in modulation amplitude. These data are provided in the Supplemental Information (SI), Fig. S1.

Figure 7 is an upgraded schematic of the CH_4 oxidation rate versus O_2 concentration that we communicated in our recent work [22]. A nonmonotonic CH_4 oxidation rate dependence was reported by Chin et al. [31] for $\text{Pt}/\text{Al}_2\text{O}_3$ powder catalyst while Bugosh et al. [32] reported a nonmonotonic CH_4 conversion dependence on O_2 feed concentration for a $\text{Pt}+\text{Pd}/\text{Al}_2\text{O}_3$ monolith catalyst. The concentration giving the maximum approaches $\text{O}_2/\text{CH}_4 = 2$ as the temperature increases [32]. Kang et al. reaffirmed the conversion versus O_2 concentration dependence [22]. This rate schematic is a convenient way to demonstrate the response of the catalyst during lean-rich modulation. To highlight, the schematic depicts the nonmonotonic CH_4 oxidation rate dependence on O_2 concentration. This includes a distinct maximum at intermediate O_2 concentration that is below the stoichiometric level required for complete CH_4 oxidation. The impact of feed switching between lean and rich is captured in the schematic by drawing a chord that connects the two extremes in CH_4 oxidation rate. Switching the feed at a prescribed frequency between a high O_2 concentration, low-rate

state and a low O_2 concentration, high rate state gives an instantaneous rate that lies along the chord. The cycle-average rate along the chord exceeds the cycle average of the instantaneous rate gotten by moving back and forth along the steady-state rate curve. Very slow switching between the same two O_2 concentration limits would give a cycle average rate corresponding to an average rate weighted by the duty cycles of the lean and rich operation. We conjectured in [22] that the modulation enables an optimal oxygen surface coverage on the Pt/Pd that maximizes the rate of CH_4 activation; Chin et al. [31] have posited that the breaking of the first C-H bond is enabled by CH_4 adsorption onto a $X + O-X$ dual site where X denotes an empty site.

The schematic illustrates how systematic variation in the modulation amplitude can lead to changes in the oxidation rate. The steady-state, time-invariant feed composition corresponds to $A = 0$. For an O_2 feed concentration given by $\langle C_{O_2} \rangle$, the steady-state rate is $R_{ss}\{\langle C_{O_2} \rangle\}$. Further, at an unbounded cycle frequency ($f \rightarrow \text{infinity}$), the lean and rich feeds become mixed and the rate should also approach $R_{ss}\{\langle C_{O_2} \rangle\}$. In the other extreme of a very slow frequency ($f \rightarrow 0$), the cycle average rate is given by the weighted-average $R_{w,d}\{\langle O_2 \rangle\} = d R\{C_{O_2,l}\} + (1 - d) R\{C_{O_2,r}\}$ where d is the duty cycle fraction of the lean feed; the schematic shows $R_{w,0.5}$. For a given rate curve there is an optimal A that maximizes $R_{w,d}$. As A is increased at a fixed, bounded frequency, the achieved rate is given by a pseudo steady state rate given by R_{pss} which may exceed $R_{w,d}$ at a given O_2 concentration $\{\langle O_2 \rangle\}$. As A is increased from 0 this is indicated by the series of chords labeled A_1 , A_2 , and so on. The transient rate at the left (richer) endpoint increases significantly due to the steep increase in the rate with decreasing O_2 concentration along the negative-order branch to the right of the rate

maximum. For sufficiently high A shown, for example, by the A_4 chord, the rich-phase O_2 concentration shifts beyond the concentration corresponding to maximum rate, resulting in decreasing rate. This illustrates the measured CH_4 conversion improvements in the PGM-only catalyst as the modulation amplitude was increased from $A = 0.0$ up to $A = 0.014$ (Fig. 5), as well as the diminished performance as the amplitude was increased beyond $A = 0.014$.

Fig. 7 also schematically illustrates also how the presence of spinel is able to dampen swings in conversion; we observed this effect in data presented in Fig. 4. Because the spinel can store and release O_2 through redox chemistry, the effective λ during the rich and lean phases may be different than what the feed λ would suggest. In the schematic we depict the rate obtained for an amplitude of A without and with spinel. This is represented in the schematic by the two chords labelled PGM: A_4 and PGM+Spinel: A_4 . The presence of spinel has the effect of decreasing the effective $C_{O_2,l}$ during the lean phase and increasing the effective $C_{O_2,r}$ during the rich phase. The net effect is a steeper chord leading to a higher cycle average rate. Even these rather small effective changes in the C_{O_2} in the rich phase can result in higher cycle average rates. These changes help to explain why the PGM+Spinel does not exhibit the decreased performance at higher temperatures experienced by the PGM-Only catalyst.

The rate at intermediate values of the modulation frequency is a function of the response of the catalyst to the changing feed composition. It is useful to determine the A and f combination that gives the maximum R_{PSS} for a given feed concentration. Whether or not the rate exceeds the non-modulated rate depends on whether a surface state can be achieved that increases the CH_4 activation rate under cyclic conditions that

is not obtainable under steady-state conditions. The cycling data shown suggest an important, additional role of the spinel that cannot be encountered with the PGM-Only catalyst. We return to this point later.

3.2.3 Modulation Frequency

Modulation frequency is the third modulation parameter to be examined. Experiments were conducted to quantify the effect of frequency (f) on the PGM+Spinel performance. These UH experiments were conducted at five fixed temperatures (315, 330, 345, 370, 415 °C), three modulation amplitudes ($A = 0.007, 0.014, 0.028$), and five different frequencies ($f = 0.33, 0.25, 0.17, 0.07, 0.05$ Hz).

Figure 8 shows how frequency impacts CH_4 conversion for the PGM+Spinel catalyst at the three values of A . The black vertical bars in the figure represent the maximum and minimum instantaneous CH_4 conversion for the given experiment (i.e., as opposed to experimental fluctuations). The data show that frequency has a significant effect on catalyst performance in terms of CH_4 conversion. Immediately apparent is the enhancement in the conversion with increasing amplitude, especially at the lower temperatures. Ferri et al. [10] reported a similar enhancement trend during lean/rich switching for a Pd-based TWC. At the lowest amplitude ($A = 0.007$) and for temperatures below 415 °C the conversion is negligible. These trends reflect the results shown earlier regarding the beneficial effect of modulation. In particular, an optimal frequency exists as a function of temperature and modulation amplitude. A key finding is that for the highest temperature (415 °C), the slowest modulation ($f = 0.05$ Hz) results in the highest CH_4 conversion, a feature that is essentially independent of amplitude. On the other hand, at the highest amplitude value ($A = 0.028$), as the temperature is

decreased an intermediate frequency value in the studied range gives a maximum CH₄ conversion. For example, at 415 °C the optimal frequency is 0.05 Hz while at 330 °C the optimal frequency shifts to 0.25 Hz. Slower modulation results in more drastic swings between high and low conversions. At the two smaller amplitude values the CH₄ conversion is negligible for temperatures of 370 °C and lower.

A more detailed look at the frequency effect is revealed upon examining the CH₄ conversion at 315 °C and A = 0.028, shown in Fig. 9. At f = 0.33 Hz the CH₄ conversion is negligible (< 5%). However, a small decrease in f to 0.25 Hz results in a dramatic increase in conversion to ~40% with instantaneous values spanning the rather wide range of ~15% to ~75%. The cycle-averaged conversion is stable for over 4 hours of operation. Light-off experiments conducted at 0.25 Hz and 0.33 Hz (Figure S2) demonstrate that the slower frequency does indeed result in an earlier light-off evidenced by the T₅₀ values; i.e., T₅₀ ~ 340 °C at 0.33 Hz and 312 °C at 0.25 Hz.

Figure 10 shows the effect of frequency on the PGM-Only catalyst at two modulation amplitudes. Interestingly, in the absence of spinel, the modulation frequency has the opposite effect that it does in the presence of spinel. The A = 0.028 data show an increasing CH₄ conversion with increasing modulation frequency, particularly at higher temperatures. The A = 0.007 data show the same trend at 415 °C. At this temperature it is also noteworthy that that smaller amplitude results in higher conversion when comparing the A = 0.007 data to the A = 0.028 data.

A closer examination of the transient trends in CH₄ conversion (or concentration) provides evidence for the enhancement from the combination of modulation and spinel addition. Figure 11 shows the effect of a very slow feed modulation on conversion for

both the PGM-Only catalyst (top panel) and PGM+Spinel catalyst (bottom panel). Data for three temperatures (315, 345, 370 °C) are shown. Here the period of a complete cycle is eight minutes (480 s) seconds), 50% duty cycle lean and rich, with $\lambda_l = 1.006$ and $\lambda_r = 0.978$. While such long lean and rich periods is impractical due to CH₄ slip during the lean part of the cycle, specific transient trends become clearly evident. For each catalyst, the lean feed CH₄ conversion is <5% while the rich feed conversion is between 20% and 90%. During the lean-to-rich transition, the conversion spikes and then decreases monotonically throughout the remainder of the rich period. The intensity of the spike depends on the catalyst; i.e., presence of spinel. A second, less prominent spike occurs during the rich-to-lean transition. No spikes occurred for NO and CO during these transitions; see Figs. S3 and S4.

A comparison of the PGM-Only and PGM+Spinel catalyst data clearly show that the lean-to-rich transition is an important driver for the enhanced CH₄ conversion during modulation for the spinel-containing catalyst. The overall features of the lean-to-rich spike, transient decline, and rich-to-lean spike are common to each catalyst. Further, the magnitudes of the baseline conversion after the lean-to-rich spike are comparable for both catalysts. However, there are two notable differences. First, at a given temperature, the magnitude of the conversion spike is much more intense for the PGM+Spinel catalyst. Second, the decrease in the transient conversion after the spike is noticeably slower for the PGM+Spinel. For example, at 370 °C the instantaneous conversion takes at least 1 minute to return to ~20% of the ΔX_M . In contrast, for the PGM-Only catalyst, the spike maximum is confined to a few seconds with the conversion quickly returning to a constant level. Finally, it is noted that the data appear

as if the conversion is approaching a steady-state value by the end of the 4-minute rich period. For selected experiments we sustained the rich period for several hours. Fig. S5 shows that catalyst activity continues to deactivate over the course of several hours.

A smaller CH₄ conversion spike is seen during the rich-to-lean transition with the PGM+Spinel catalyst (e.g., at 480s in Fig 11b). The excess O₂ may quickly react with CO and H adsorbed on the PGM crystallites and also reoxidize the partially depleted MFO spinel. That the spike is less intense underscores the lower rate of CH₄ activation and oxidation under the lean conditions. Similar small spikes are seen during both the lean-to-rich and the rich-to-lean transitions in the PGM-Only sample (Fig. 11a). The absence of MFO in the PGM-Only sample explains the absence of the intense activity spikes of the PGM+Spinel catalyst. The transient features reported here have some precedence. Shi et al., reported a spike in CH₄ conversion during oxidation over a TWC during the lean-to-rich transition of feed modulation [33].

Quantification of the CH₄ conversion spike and its transient relaxation suggests that this is a key contributor of the enhanced performance of the spinel-containing Pt/Pd catalyst during modulation. Using the data shown in Fig. 11, we estimated the quantity of unreacted CH₄ in the effluent during the rich feed for both catalysts. Additionally, the quantity of unreacted CH₄ was estimated if the CH₄ conversion spike did not exist for the PGM+Spinel catalyst. Fig. S6 illustrates how this analysis was conducted while Table 3 provides the results of the analysis. At 315 °C and 345 °C, the CH₄ conversion spike accounts for ~70% of the difference in conversion between the PGM-Only and PGM+Spinel catalysts. At 370 °C, the spike accounts for well over 100% of the difference. The latter anomaly is due to the fact that the PGM+Spinel catalyst ends the

rich phase at a slightly lower conversion (39% compared to 42% for the PGM-Only catalyst). Adjusting the baseline final conversion to 42% results in the transient spike accounting for 88% of the difference between catalysts, in line with the results at other temperatures.

The results of a similar analysis provided in Table 4 estimates how much CH₄ conversion is attributed to the transient activity spike as a function of time. The transient spike at 345 °C was considered. A baseline was created, and used to estimate CH₄ conversion as if the transient spike did not exist. The difference in the actual results and these estimates were then calculated. During the entire 240s rich phase, the spike accounts for just a 5% difference in conversion. The same can be said when one looks at the first three seconds of the rich phase. However, a “sweet spot” exists at 10 seconds where the conversion spike results in a 36% difference in unreacted CH₄ present in the effluent. This condition tracks well with frequency results previously shown in Fig. 8, particularly for amplitudes of 0.014 and 0.007.

Quantifying the lean-to-rich transient conversion spike appears to be critical to understanding how the spinel enhances the CH₄ oxidation rate on the Pt-rich catalyst. We previously attributed the enhancement to the formation of a more catalytically favorable mixture of metallic and partially oxidized Pt crystallites reacting with O₂ released from the spinel. While this plays a role in catalytic activity – as seen in the pretreatment experiments in Fig. 4 – it does not fully explain how important the O₂ stored by the spinel can be for CH₄ conversion.

With this in mind, we advance the following mechanism to explain the CH₄ conversion spike over the PGM+Spinel catalyst. During the lean period, the conversion

is low and the catalyst is saturated with O₂. The PGM crystallites are likely covered with O adatoms while the spinel crystallites for the PGM+Spinel catalyst are fully oxidized. The conversion on Pt is negligible in this temperature range due to adsorbed oxygen inhibition. [Remark: We acknowledge that there are likely differences in the Pt and Pd but we need not make a distinction here. For example, lean CH₄ oxidation is more effective on Pd than Pt due to the formation of PdO [16]. However, with the large excess of Pt (19:1 Pt:Pd mass ratio), the contribution by Pd is limited.] Now, upon the switch to the O₂-deficient rich feed, CH₄ reacts with adsorbed O, creating vacant PGM sites. This leads to an increase in the reaction rate; as described earlier, the CH₄ activation on Pt is fastest on the dual site comprising O-Pt + Pt. [31]. However, the O₂/CH₄ is less than the deep oxidation stoichiometric ratio of 2. As a result, oxidation products will be a mixture of CO, H₂, CO₂, and H₂O. That the intensity of the CH₄ conversion spike is much higher for the PGM+Spinel suggests an important role of the spinel during the lean-to-rich feed switch. Zhou et al. [24] recently reported the dynamic oxygen storage capacity (DOSC) of the same MFO spinel and found that the reduction of MFO occurs through a sequential, two-step process. Oxygen in the surface layer of the MFO crystallites is removed during the first few seconds through reaction with CO and H₂. This is followed by the gradual removal of the bulk oxygen in a diffusion-controlled reaction.

Thus, we propose that partial oxidation products CO and H₂ formed during the lean-to-rich transition are rapidly consumed through reaction with oxygen from the spinel crystallites. This continues until all of the oxygen in the surface layer of the MFO crystallites is consumed, a process that, as Zhou et al. found, occurs in the first few seconds following the shift to rich conditions [24]. Once this O₂ is depleted, CH₄

conversion decreases as bulk O₂ from the MFO is consumed. The shift in consumption of surface O₂ to bulk O₂ would correspond with the sharp spike followed by the slower deactivation in CH₄ conversion seen immediately after the lean-to-rich transition. The removal of CO and H₂ cleanses the PGM crystallites, enabling a sustained higher CH₄ conversion rate.

This explanation requires that CO inhibits CH₄ partial oxidation or steam reforming. There is some literature evidence to support CO inhibiting partial oxidation. Jakobsen et al., reported inhibition of SMR over Rh-based catalysts [34]. Furthermore, experiments conducted at UH have also seen evidence of this inhibition over the PGM+Spinel catalyst. The addition of 2000 ppm to a feed of 1500ppm CH₄, 10% H₂O, and balance N₂ increased the T₅₀ of CH₄ conversion by 80 °C, from 370 °C to 450 °C. The further addition of another 2000 ppm (4000 ppm CO total) increased the T₅₀ to 477 °C. These findings will be further explored in an upcoming paper. Suffice to say, CO certainly appears to inhibit SMR.

These experimental findings and the earlier results of Shi et al. [12] clearly show that an oxygen storage material (OSM) is needed to enable enhanced CH₄ conversion during the lean-to-rich switch. Shi et al. attributed the spike in conversion to an important role of oxygen supply by an unidentified OSM in their catalyst. Assuming the material was CeO₂, then the mechanism is not likely to be much different than what we are proposing, i.e. CO and H₂ generated by SMR and/or partial oxidation react with oxygen supplied by the OSM. Further, Ferri et al. [10] reported conversion enhancement for a Pd-based TWC with a Pd loading of 56 g/ft³ containing Ce and Zr oxides but with unspecified loadings. The MFO spinel may be more active due to its

intrinsic higher dynamic oxygen storage capacity. As Zhou et al. [24] have shown, the MFO spinel provides sufficient oxygen during the first few seconds for CO and H₂ oxidation, avoiding the need for bulk oxygen in fast modulation. Nonetheless, additional research is needed to compare the spinel and CZO materials in the context of methane oxidation.

Experiments examining catalytic activity during transitions between lean and rich feed conditions were repeated without water in the system and with O₂ concentrations adjusted to maintain the same rich and lean λ values (using eqn. (1)). In the lean phase, O₂ was decreased from 7900 ppm to 7650 ppm, while in the rich phase O₂ was increased from 3400 ppm to 4550 ppm. The CH₄ conversion plots for the PGM+Spinel catalyst are shown in Fig S7. In the absence of H₂O, a higher temperature is needed to obtain an adequate CH₄ conversion. Moreover, the transient activity spike is not observed. These results show that the transient spike needs both an OSM in the catalyst and the presence of water in the feed. The need for H₂O in the feed supports our earlier argument that transient activity spike is related to SMR. In our earlier work, we showed that total O₂ consumption occurs well before complete CH₄ oxidation, necessitating reaction with H₂O to achieve higher conversion [22]. In data to be reported elsewhere, we show that CH₄ reacts with H₂O through SMR at comparable temperatures to total oxidation over PGM+Spinel catalysts.

Finally, it is noted that the transient conversion spike is in addition to the performance gains obtained from feed modulation. The feed modulation amplitude experiments had frequencies between 0.33 Hz (Fig. 6 & S1) and 1 Hz (Fig 5); these frequencies are too fast to capture the increased performance resulting from the lean-

to-rich transition. The boost in CH₄ conversion, through enhanced partial oxidation or SMR resulting from CO and H₂ reacting with spinel-stored oxygen, suggest that the PGM+Spinel catalyst can achieve CH₄ conversions above what is possible through feed modulation on PGM-Only catalyst alone. The transient spike also explains the existence of the apparent optimal feed modulation frequency. That is, by slowing the feed modulation frequency, a larger portion of the high-activity transient spike is captured in the rich phase. It is therefore possible to push the cycle-average FWC performance even higher than what we reported in our earlier study [22].

4. Conclusions

Catalyst design and operating parameters were systematically varied in order to better understand and optimize the dual-layer Pt/Pd+Spinel FWC catalyst performance for coupled CH₄ and NO conversion. The data show the FWC performance requires separation of the MFO spinel from the PGM in order to avoid detrimental loss in activity at high methane conversion. Intermediate alumina layer experiments demonstrate that the distance between the two layers is irrelevant during practical applications. Taken together, these experiments confirm that MFO Spinel operates through a different mechanism than traditional OSM materials such as ceria and ceria-zirconia.

Modulation amplitude, modulation frequency, and feed composition effects were investigated. The data show that large modulation amplitudes inhibit CH₄ conversion at higher temperatures with the PGM-Only catalyst. This decrease in performance is not encountered when the catalyst contains spinel. The effects of modulation amplitude are

tied to the nonmonotonic rate dependence of CH₄ oxidation on O₂ concentration, along with the efficient dynamic oxygen storage and release property ability of the MFO to mitigate swings in O₂ during feed modulation. Varied frequency experiments show that an optimal frequency exists for the PGM+Spinel catalyst. That frequency is a function of the other feed parameters including temperature and amplitude; for example, experiments at lower modulation amplitudes show that even slower frequencies are best. The PGM-Only catalyst has a similar optimal frequency at lower temperatures, but requires a higher frequency at higher temperatures. This underscores the important, modifying role of the spinel's oxygen storage capacity.

Systematic, low frequency experiments reveal a noted transient spike in the CH₄ conversion during the lean-to-rich transition over the PGM+Spinel catalyst, an apparent key cause for the enhanced catalytic activity. We conjecture that this transient spike is a result of the MFO spinel removing partial oxidation and steam reforming products, CO and H₂, from the gas stream via oxidation from the stored O₂ and gaseous H₂O, thereby driving further CH₄ steam reforming.

Finally, this study shows that feed parameters need to be tuned to provide maximum methane oxidation activity and conversion efficiency. The optimal operating parameters appear to be a slightly rich, modulated feed, with a sufficiently large modulation amplitude and a low modulation frequency (~ 0.2 Hz). Future research involving experiments and modeling will focus on furthering our understanding of the underlying mechanism of enhanced methane oxidation activity through modulation and spinel addition.

Acknowledgements

The authors gratefully acknowledge DOE Vehicle Technologies Office (project award number: DE-EE0008332) for funding. The supply of catalysts from CDTi (Oxnard, CA) is also acknowledged.

List of References

- [1] E.O. of Transportation, Fast Facts: U.S. Transportation Sector Greenhouse Gas Emissions, 1990-2017 (EPA-420-F-19-047, June 2019), 2019. <https://nepis.epa.gov/Exe/ZyPDF.cgi?Dockey=P100WUHR.pdf> (accessed June 28, 2020).
- [2] F. Arosio, S. Colussi, G. Groppi, A. Trovarelli, Regeneration of S-poisoned Pd/Al₂O₃ catalysts for the combustion of methane, *Catal. Today*. 117 (2006) 569–576. doi:10.1016/J.CATTOD.2006.06.006.
- [3] A. Raj, Methane emission control, *Johnson Matthey Technol. Rev.* 60 (2016) 228–235. doi:10.1595/205651316X692554.
- [4] P.L. Silveston, Automotive exhaust catalysis under periodic operation, *Catal. Today*. (1995). doi:10.1016/0920-5861(95)00107-Q.
- [5] H. Muraki, K. Yokota, Y. Fujitani, Nitric oxide reduction performance of automotive palladium catalysts, *Appl. Catal.* (1989). doi:10.1016/S0166-9834(00)80268-7.
- [6] J.H.B.J. Hoebink, J.M.A. Harmsen, M. Balenovic, A.C.P.M. Backx, J.C. Schouten, Automotive exhaust gas conversion: From elementary step kinetics to prediction of emission dynamics, *Top. Catal.* 16–17 (2001) 319–327. doi:10.1023/A:1016609031602.
- [7] A.T. Gremminger, H.W. Pereira de Carvalho, R. Popescu, J.-D. Grunwaldt, O. Deutschmann, Influence of gas composition on activity and durability of bimetallic Pd-Pt/Al₂O₃ catalysts for total oxidation of methane, *Catal. Today*. 258 (2015) 470–480. doi:10.1016/J.CATTOD.2015.01.034.
- [8] A.K. Datye, J. Bravo, T.R. Nelson, P. Atanasova, M. Lyubovsky, L. Pfefferle, Catalyst microstructure and methane oxidation reactivity during the Pd↔PdO transformation on alumina supports, *Appl. Catal. A Gen.* 198 (2000) 179–196. doi:10.1016/S0926-860X(99)00512-8.
- [9] D. Bounechada, G. Groppi, P. Forzatti, K. Kallinen, T. Kinnunen, Effect of periodic lean/rich switch on methane conversion over a Ce-Zr promoted Pd-Rh/Al₂O₃ catalyst in the exhausts of natural gas vehicles, *Appl. Catal. B Environ.*

- 119–120 (2012) 91–99. doi:10.1016/j.apcatb.2012.02.025.
- [10] D. Ferri, M. Elsener, O. Kröcher, Methane oxidation over a honeycomb Pd-only three-way catalyst under static and periodic operation, *Appl. Catal. B Environ.* 220 (2018) 67–77. doi:https://doi.org/10.1016/j.apcatb.2017.07.070.
- [11] J. Gong, J. Pihl, D. Wang, M.-Y. Kim, W.P. Partridge, J. Li, M. Cunningham, K. Kamasamudram, N. Currier, A. Yezerets, O₂ dosage as a descriptor of TWC performance under lean/rich dithering in stoichiometric natural gas engines, *Catal. Today.* (2020). doi:10.1016/J.CATTOD.2020.02.022.
- [12] X. Shi, R. Seiser, J.-Y. Chen, R. Dibble, R. Cattolica, Fuel-Dithering Optimization of Efficiency of TWC on Natural Gas IC Engine, *SAE Int. J. Engines.* 8 (2015) 1246–1252. doi:10.4271/2015-01-1043.
- [13] K. Persson, A. Ersson, K. Jansson, J.L.G. Fierro, S.G. Järås, Influence of molar ratio on Pd-Pt catalysts for methane combustion, *J. Catal.* 243 (2006) 14–24. doi:10.1016/j.jcat.2006.06.019.
- [14] G. Lapisardi, L. Urfels, P. Gélin, M. Primet, A. Kaddouri, E. Garbowski, S. Toppi, E. Tena, Superior catalytic behaviour of Pt-doped Pd catalysts in the complete oxidation of methane at low temperature, *Catal. Today.* 117 (2006) 564–568. doi:10.1016/j.cattod.2006.06.004.
- [15] M.S. Wilburn, W.S. Epling, Sulfur deactivation and regeneration of mono- and bimetallic Pd-Pt methane oxidation catalysts, *Appl. Catal. B Environ.* 206 (2017) 589–598. doi:10.1016/J.APCATB.2017.01.050.
- [16] P. Gélin, M. Primet, Complete oxidation of methane at low temperature over noble metal based catalysts: a review, *Appl. Catal. B Environ.* 39 (2002) 1–37. doi:10.1016/S0926-3373(02)00076-0.
- [17] S. Rood, S. Eslava, A. Manigrasso, C. Bannister, Recent advances in gasoline three-way catalyst formulation: A review, *Proc. Inst. Mech. Eng. Part D J. Automob. Eng.* 234 (2020) 936–949. doi:10.1177/0954407019859822.
- [18] M. Ozawa, Role of cerium-zirconium mixed oxides as catalysts for car pollution: A short review, *J. Alloys Compd.* 275–277 (1998) 886–890. doi:10.1016/S0925-8388(98)00477-0.
- [19] R. Möller, M. Votsmeier, C. Onder, L. Guzzella, J. Gieshoff, Is oxygen storage in three-way catalysts an equilibrium controlled process?, *Appl. Catal. B Environ.* 91 (2009) 30–38. doi:10.1016/j.apcatb.2009.05.003.
- [20] D. Fino, S. Solaro, N. Russo, G. Saracco, V. Specchia, Catalytic removal of methane over thermal-proof nanostructured catalysts for CNG engines, in: *Top. Catal.*, 2007. doi:10.1007/s11244-007-0223-x.
- [21] D. Fino, N. Russo, G. Saracco, V. Specchia, CNG engines exhaust gas treatment via Pd-Spinel-type-oxide catalysts, *Catal. Today.* (2006). doi:10.1016/j.cattod.2006.06.003.

- [22] S.B. Kang, K. Karinshak, P.W. Chen, S. Golden, M.P. Harold, Coupled methane and NO_x conversion on Pt + Pd/Al₂O₃ monolith: Conversion enhancement through feed modulation and Mn_{0.5}Fe_{2.5}O₄ spinel addition, *Catal. Today*. (2020). doi:10.1016/j.cattod.2020.02.039.
- [23] A. Trovarelli, *Catalysis Reviews Catalytic Properties of Ceria and CeO₂-Containing Materials* (1996). doi:10.1080/01614949608006464.
- [24] Z. Zhou, M.P. Harold, D. Luss, Enhanced NO, CO and C₃H₆ conversion on Pt/Pd catalysts: Impact of oxygen storage material and catalyst architecture, *Catal. Today*. 360 (2021) 375–387. doi:10.1016/j.cattod.2020.01.026.
- [25] C. Bozo, N. Guilhaume, J.-M. Herrmann, Role of the Ceria–Zirconia Support in the Reactivity of Platinum and Palladium Catalysts for Methane Total Oxidation under Lean Conditions, *J. Catal.* 203 (2001) 393–406. doi:10.1006/JCAT.2001.3320.
- [26] M. Bhattacharya, M.P. Harold, V. Balakotaiah, Mass-transfer coefficients in washcoated monoliths, *AIChE J.* 50 (2004) 2939–2955. doi:10.1002/aic.10212.
- [27] M. Bhattacharya, M.P. Harold, V. Balakotaiah, Shape normalization for catalytic monoliths, *Chem. Eng. Sci.* 59 (2004) 3737–3766. doi:10.1016/j.ces.2004.02.020.
- [28] K.A. Karinshak, P. Lott, M.P. Harold, O. Deutschmann, In situ Activation of Bimetallic Pd–Pt Methane Oxidation Catalysts, *ChemCatChem*. (2020). doi:10.1002/cctc.202000603.
- [29] Y. Mahara, K. Murata, K. Ueda, J. Ohyama, K. Kato, A. Satsuma, Time Resolved in situ DXAFS Revealing Highly Active Species of PdO Nanoparticle Catalyst for CH₄ Oxidation, *ChemCatChem*. 10 (2018) 3353–3353. doi:10.1002/cctc.201801246.
- [30] H. Xiong, K. Lester, T. Ressler, R. Schlögl, L.F. Allard, A.K. Datye, Metastable Pd ⇌ PdO Structures During High Temperature Methane Oxidation, *Catal. Letters*. 147 (2017). doi:10.1007/s10562-017-2023-7.
- [31] Y.H. Chin, C. Buda, M. Neurock, E. Iglesia, Reactivity of chemisorbed oxygen atoms and their catalytic consequences during CH₄-O₂ catalysis on supported Pt clusters, *J. Am. Chem. Soc.* (2011). doi:10.1021/ja202411v.
- [32] G.S. Bugosh, V.G. Easterling, I.A. Rusakova, M.P. Harold, Anomalous steady-state and spatio-temporal features of methane oxidation on Pt/Pd/Al₂O₃ monolith spanning lean and rich conditions, *Appl. Catal. B Environ.* 165 (2015) 68–78. doi:10.1016/J.APCATB.2014.09.058.
- [33] S. Zhang, J. Shan, L. Nie, L. Nguyen, Z. Wu, F. (Feng) Tao, In situ studies of surface of NiFe₂O₄ catalyst during complete oxidation of methane, *Surf. Sci.* 648 (2016) 156–162. doi:10.1016/J.SUSC.2015.12.011.
- [34] J.G. Jakobsen, M. Jakobsen, I. Chorkendorff, J. Sehested, Methane steam

reforming kinetics for a rhodium-based catalyst, Catal. Letters. (2010).
doi:10.1007/s10562-010-0436-7.

PGM+Spinel		Washcoat Loading
PGM / Al ₂ O ₃ (Pt:Pd :: 19:1, 30g/ft ³)		1.64 g/in ³
Spinel / Al ₂ O ₃ (25wt.% Mn _{0.5} Fe _{2.5} O ₄)		1.64 g/in ³
Cordierite		
PGM-Only		
PGM / Al ₂ O ₃ (Pt:Pd :: 19:1, 30g/ft ³)		1.64 g/in ³
Alumina		0.98 g/in ³
Cordierite		
PGM+Spinel (Single Layer)		
PGM (Pt:Pd :: 19:1, 30g/ft ³) & Spinel (25wt.% Mn _{0.5} Fe _{2.5} O ₄) / Al ₂ O ₃		1.64 g/in ³
Cordierite		
PGM-Only (Single Layer)		
PGM / Al ₂ O ₃ (Pt:Pd :: 19:1, 30g/ft ³)		1.64 g/in ³
Cordierite		
PGM+Spinel (Intermediate Layer)		
PGM / Al ₂ O ₃ (Pt:Pd :: 19:1, 30g/ft ³)		0.98 g/in ³
Alumina		0, 0.66, 0.98, or 1.31 g/in ³
Spinel / Al ₂ O ₃ (25wt.% Mn _{0.5} Fe _{2.5} O ₄)		0.98 g/in ³
Cordierite		

Figure 1. Schematic of Catalysts (Dual-Layer PGM+Spinel, Dual-Layer PGM-Only, Single-Layer PGM+Spinel, Single-Layer PGM-Only, & Intermediate Layer catalysts)

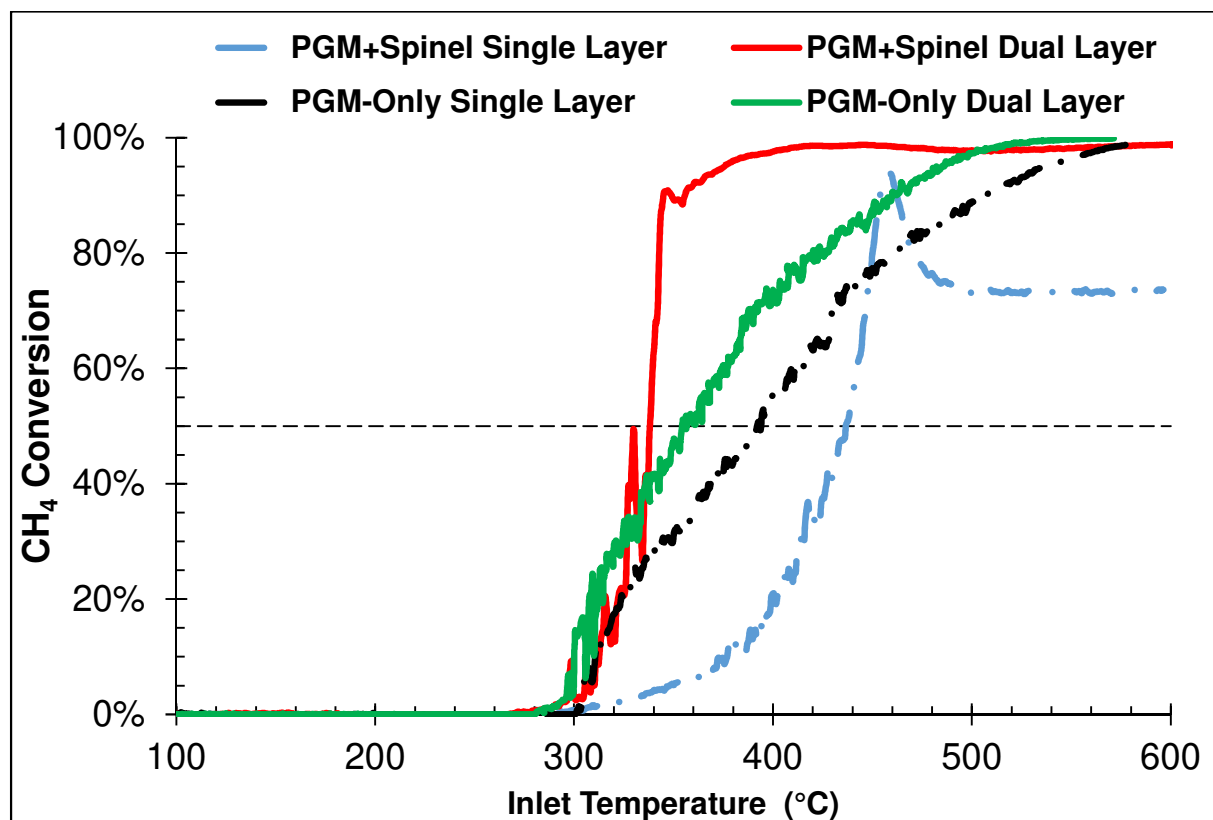


Figure 2. Single vs. Dual Layer results for the PGM+Spinel and PGM-Only catalysts. Light-Off curves conducted at $\Delta T = 40$ °C/min under CDTI Modulation feed conditions. Horizontal line shows 50% conversion.

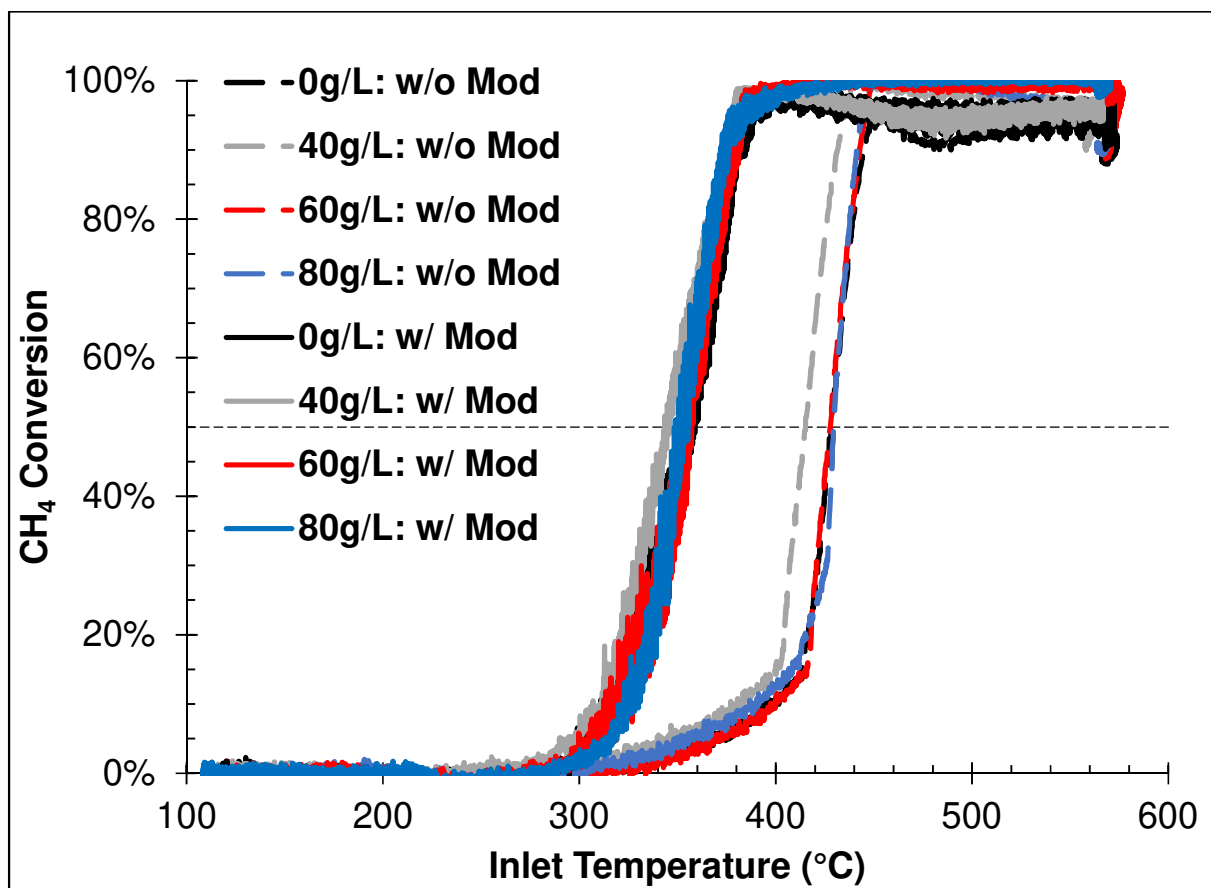


Figure 3. CH₄ conversion from experiments conducted with catalysts with various intermediate layers (0 to 80 g/L) of Al₂O₃. Light-off ramps performed at $\Delta T = 10$ °C/min under Full Feed conditions with and without modulation. Horizontal line shows 50% conversion.

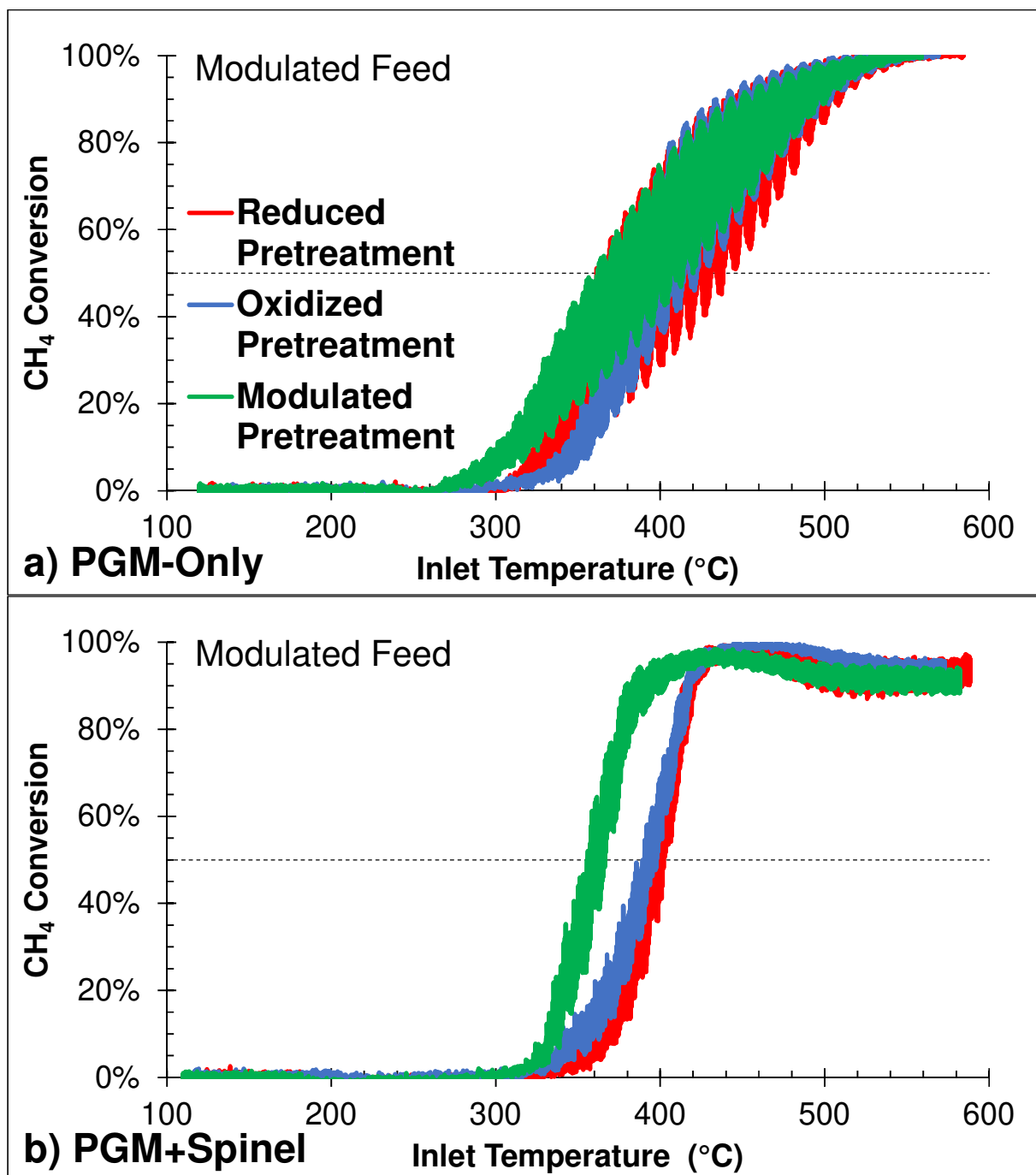


Figure 4. CH₄ conversion as affected by different pretreatments for the a) PGM-Only and b) PGM+Spinel catalysts. Light-off ramps performed at $\Delta T = 10$ °C/min under Full Feed modulated conditions. Pretreatment conditions are listed in Table 1. Horizontal line shows 50% conversion.

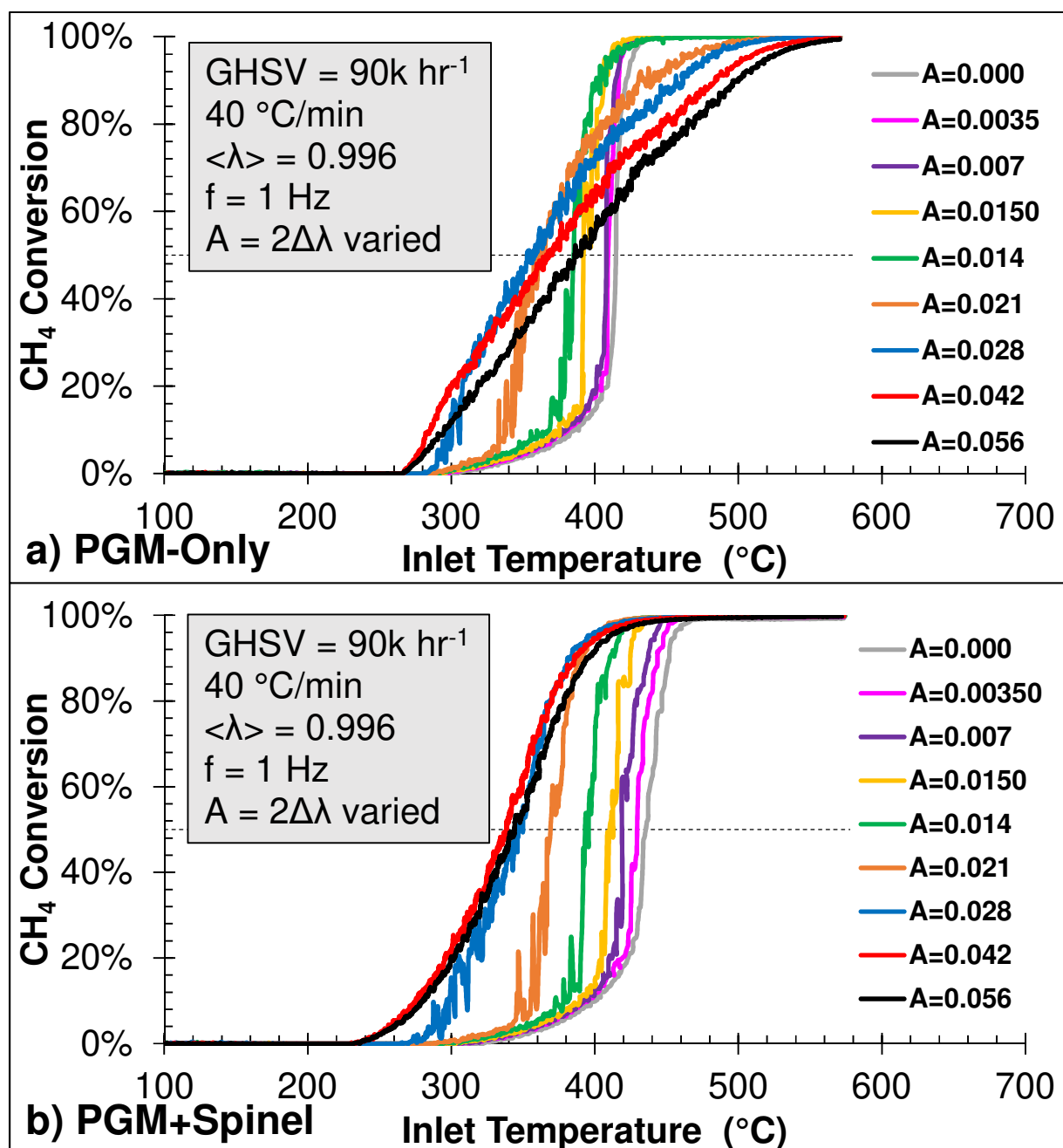


Figure 5. Experiments showing the effects of varying oscillation amplitude for the a) PGM-Only and b) PGM+Spinel catalysts. Light-off ramps performed at $\Delta T = 40$ °C/min under CDTI modulated conditions. Horizontal line shows 50% conversion.

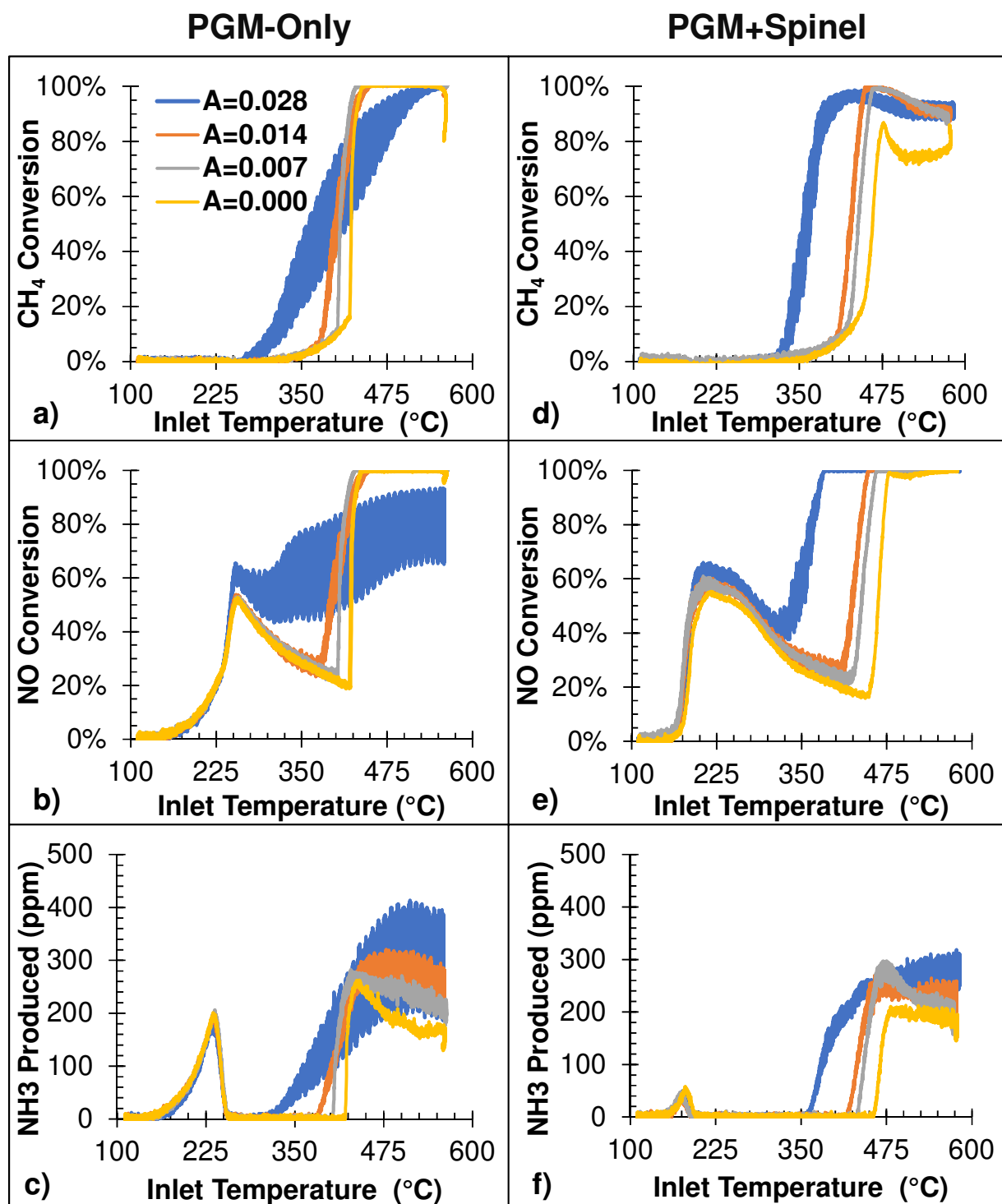


Figure 6. Experiments showing the effects of varying oscillation amplitude. Light-off ramps performed at $\Delta T = 10$ °C/min under Full Feed modulated conditions.

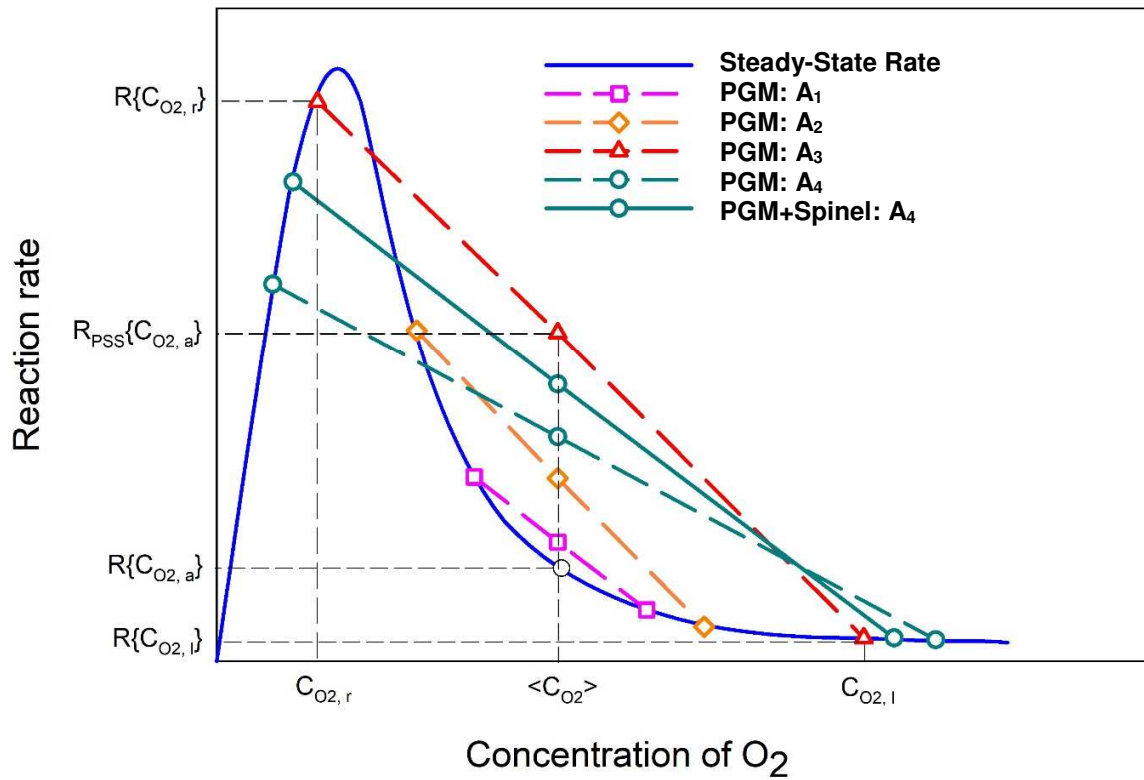


Figure 7. Schematic showing dependence of methane oxidation rate on feed O_2 concentration from previous paper [22]. The schematic shows how raising oscillation amplitude too high can inhibit CH_4 rate, and how the addition of MFO can mitigate this issue.

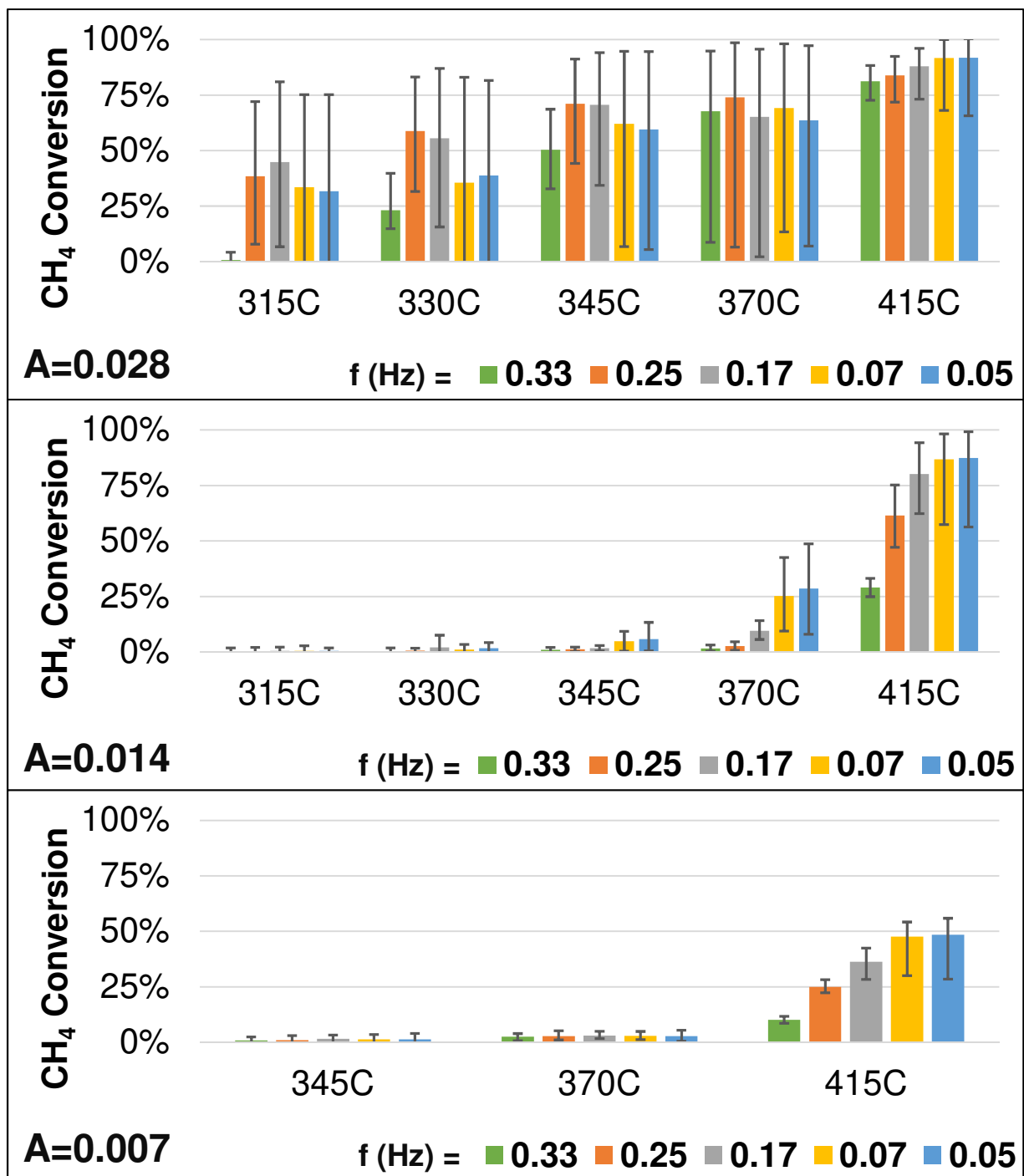


Figure 8. Effects of varying oscillation frequency on CH₄ conversion from the PGM+Spinel catalyst. Experiments conducted at steady temperatures under Full Feed modulated conditions.

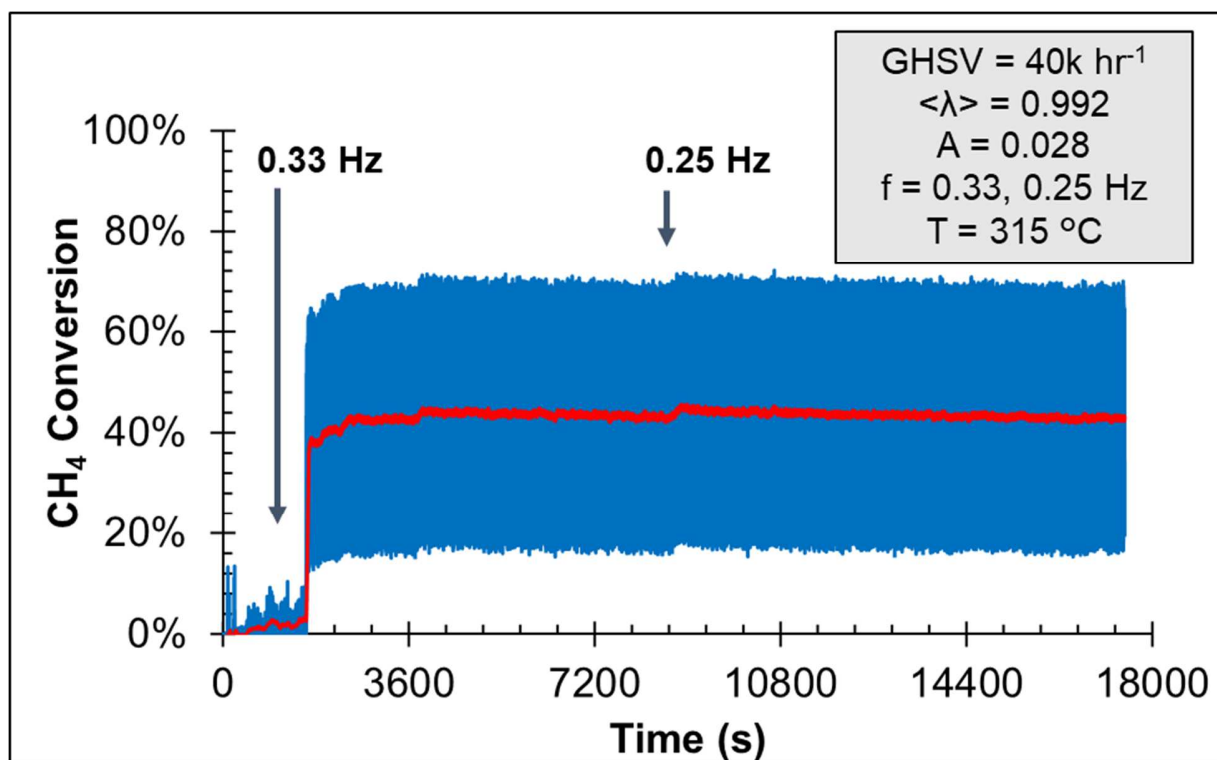


Figure 9. Long-term stability of the PGM+Spinel catalyst under slower frequency, Full Feed modulation conditions at 315 °C. Red line shows average conversion while blue line shows minimum and maximum conversions.

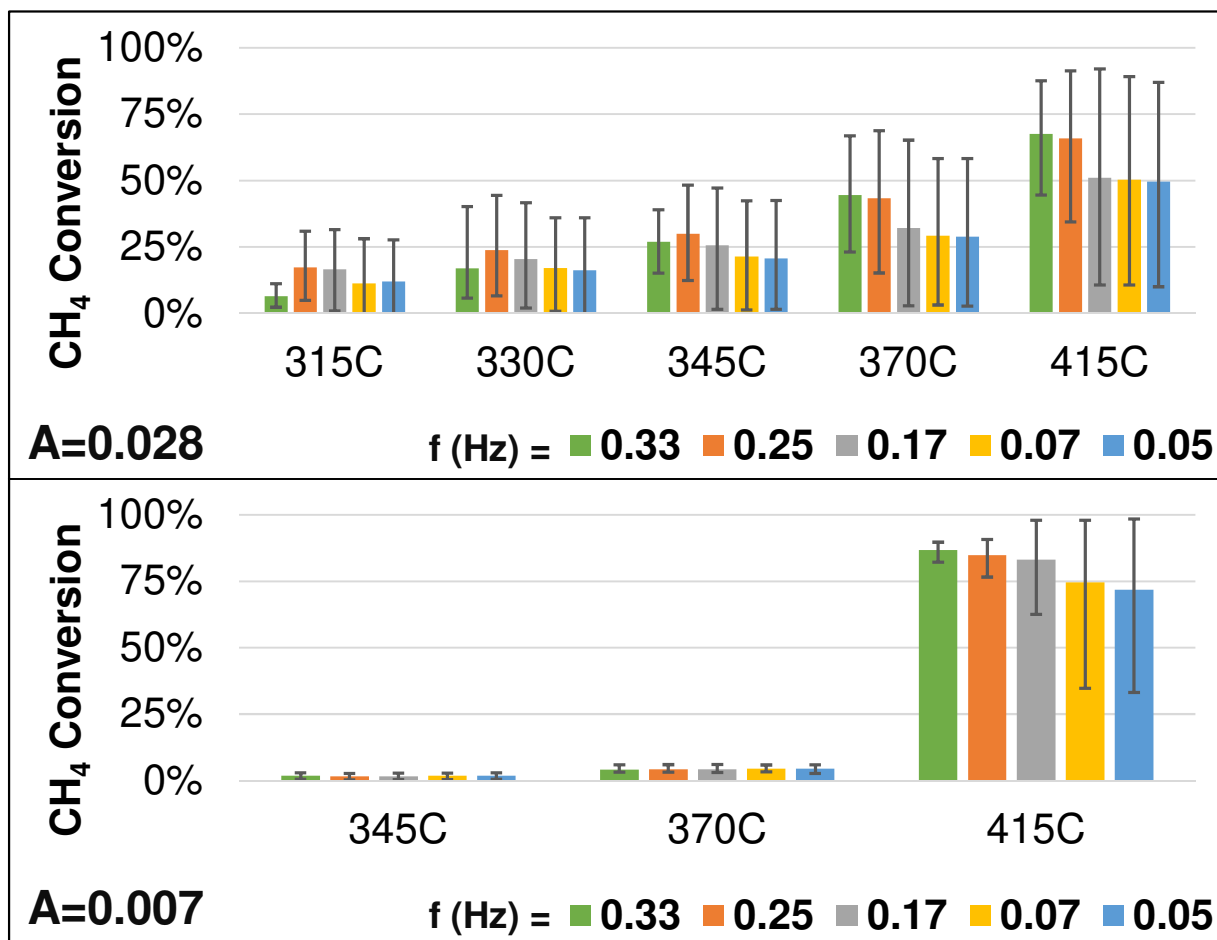


Figure 10. Effects of varying oscillation frequency on CH_4 conversion from the PGM-Only catalyst. Experiments conducted at steady temperatures under Full Feed modulated conditions.

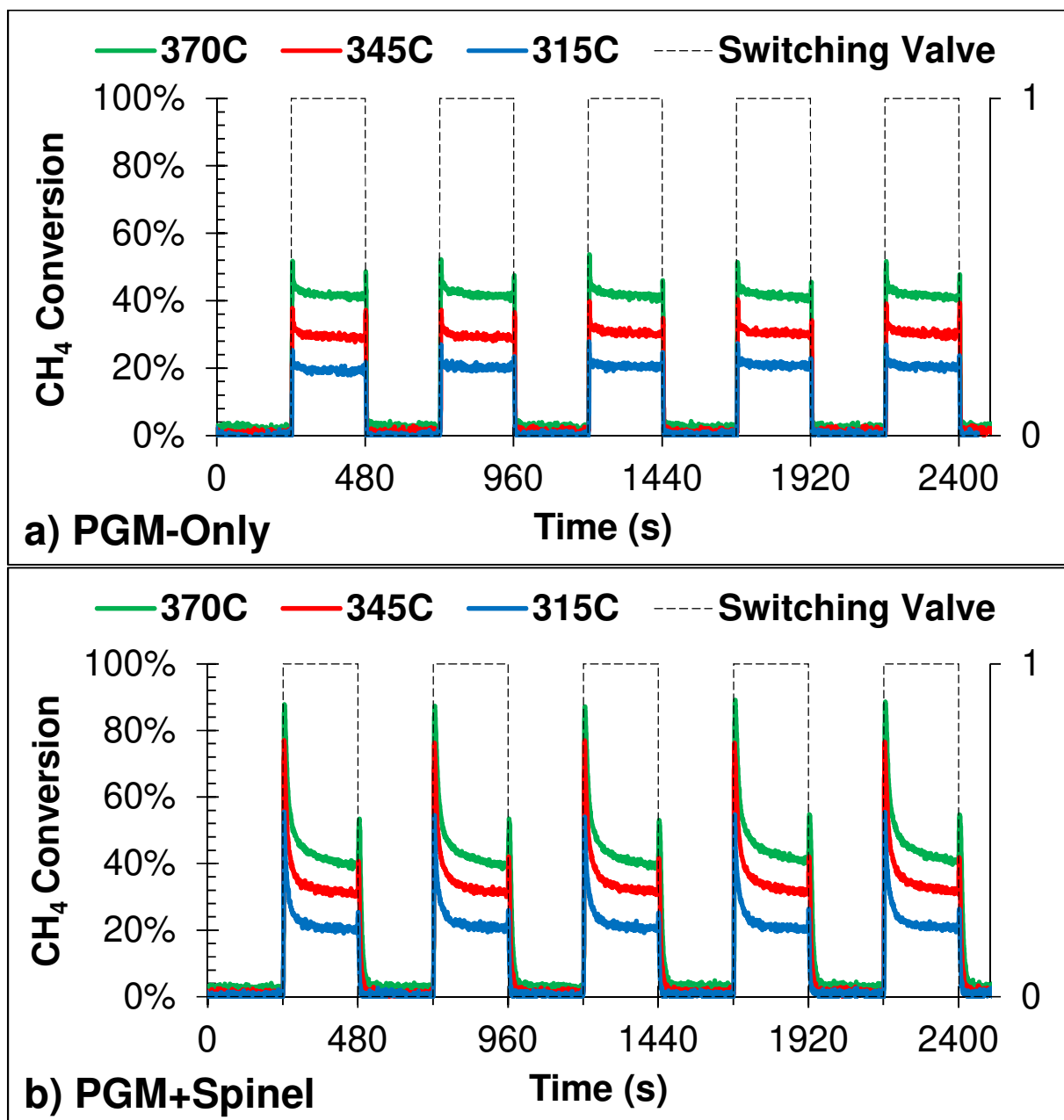


Figure 11. Examining the CH₄ conversion during lean-to-rich and rich-to-lean transitions of the a) PGM-only and b) PGM+Spinel catalysts. Experiments carried out under Full Feed modulated conditions.

Table 1. Pretreatment Conditions. Pretreatments run for thirty minutes at 525 °C.

Feed Conditions	Lambda	CH ₄	CO	H ₂	NO	O ₂
Reduced Pretreatment (Time-Invariant Feed)	$\lambda = 0.992$	1500 ppm	8000 ppm	1000 ppm	1000 ppm	5650 ppm
Oxidized Pretreatment	$\lambda = 1.038$	-	-	-	-	5650 ppm
Modulation Pretreatment	$\langle \lambda \rangle = 0.992$ (0.978-1.006 at 0.33 Hz)	1500 ppm	8000 ppm	1000 ppm	1000 ppm	7900 ppm (1.5 sec) / 3400 ppm (1.5 sec)
CDTI Pretreatment	$\langle \lambda \rangle = 0.996$ (0.982-1.01 at 1 Hz)	1500 ppm	8000 ppm	2000 ppm	1000 ppm	8900 ppm (0.5 sec) / 4500 ppm (0.5 sec)

Each pretreatment also has 10% CO₂, 10% H₂O, and balance N₂.

Table 2. Feeds composition with and without modulated feed condition.

	Full Feed w/o modulation	Full Feed w/ modulation	CDTI Feed w/o modulation	CDTI Feed w/ modulation
	$\lambda = 0.992$	$\langle \lambda \rangle = 0.992$ (0.978-1.006 at varying Hz)	$\lambda = 0.996$	$\langle \lambda \rangle = 0.996$ (0.982-1.009 at 1 Hz)
CH₄	1500 ppm	1500 ppm	1500 ppm	1500 ppm
CO	8000 ppm	8000 ppm	8000 ppm	8000 ppm
H₂	1000 ppm	1000 ppm	2000 ppm	2000 ppm
NO	1000 ppm	1000 ppm	1000 ppm	1000 ppm
CO₂	10%	10%	10%	10%
H₂O	10%	10%	10%	10%
O₂	5650 ppm	7900 ppm / 3400 ppm	6900 ppm	8900 ppm/ 4500 ppm @ 1 Hz

Table 3. Quantification of how much the lean-to-rich transient spike boosts CH₄ conversion between PGM+Spinel and PGM-Only catalysts.

Temp	PGM-Only Rich Phase Unreacted CH ₄ (ppm·s)	PGM+Spinel Rich Phase Unreacted CH ₄ (ppm·s)	Estimated PGM+Spinel with no Transient Spike (ppm·s)	Difference between no spike and transient spike present (ppm·s)	Effects of Spinel not from Transient Spike	% of Spinel Boost Attributed to the transient Spike
315 °C	313707	300923	310365	9441	3343	74%
345 °C	274759	254855	269178	14323	5581	72%
370 °C	227338	216363	236788	20425	-9450	186%
370 °C*	227338	216363	226030	9667	1308	88%

*The final column has an adjusted baseline to put the final PGM+Spinel conversion at 42% (from 39%), the same as the PGM-Only catalyst at that level.

Table 4. Quantification of how the lean to rich transient spike affects conversion as a function of rich period duration over the PGM+Spinel catalyst at 345 °C.

Freq. (Hz)	0.167	0.125	0.0625	0.05	0.0167	0.0083	0.001
Rich Period	3 s	4 s	8 s	10 s	30 s	60 s	240 s
Data	4111	4642	6441.6	7640.3	24642.4	54988.1	254855
Estimation	4308	5398	9758	11938	33738	66438	269178
% Diff	4.6	14.0	34.0	36.0	27.0	17.2	5.3

